ORIGINAL ARTICLE

Crystallization kinetics of lithium–aluminum–germanium–phosphate glass doped with MgO using a non-isothermal method

Jae-Min Cha[1] · Liyu Liu[2] · Hyun-Joon Lee[2] · Won-Jong Jeong[2] · Hyung-Sik Lim[2] · Bong-Ki Ryu[2]

Abstract

This study examines the effect of MgO content on the crystallization behavior of lithium–aluminum–germanium–phosphate glasses using differential thermal analysis (DTA), X-ray diffraction (XRD), and scanning electron microscopy (SEM). The DTA results show that the crystallization temperature decreased with an increasing MgO content and increased with increasing heating rates. The crystalline phase is investigated with XRD to determine the presence of $LiGe_2(PO_4)_3$ and $LiMgPO_4$. The activation energy, as the kinetic parameter, is obtained using the Kissinger and Marotta methods, and the SEM results confirm the change in the Avrami index with the MgO content.

Keywords Crystallization kinetics · Differential thermal analysis · Non-isothermal process

1 Introduction

Researchers have been developing glass–ceramic materials as solid electrolytes in all-solid-state lithium-ion batteries. Solid-state lithium-ion batteries have attracted significant interest as potentially safe and stable energy storage systems. All-solid-state lithium-ion batteries, as a next-generation energy storage technology, use solid-state electrolytes instead of liquid electrolytes and have shown great potential to provide higher energy density and better safety than current commercial lithium-ion batteries [1]. There are many potential solid electrolyte, and NASICON structures having the general structure $LiM_2(PO_4)_3$ are among the most promising oxide-based solid electrolytes. Especially, Ge-based $LiM_2(PO_4)_3$-doped Al, $Li_{1+x}Ge_{2-x}Al_xP_3O_{12}$ (LAGP), has attracted interest because of its superior chemical stability and wide electrochemical window [2]. Numerous studies have been conducted on the composition, manufacturing method, and coating of solid electrolytes used in all-solid-state lithium-ion batteries [3–9]. Because lattice defects in a crystalline solid electrolyte form a path through which lithium ions can move, crystallized glass, rather than an amorphous state glass, is used as the solid electrolyte [10, 11]. These solid electrolytes are manufactured using the crystallization of glass, and various studies have focused on improving the performance of solid electrolytes. The mechanical and electrical properties of solid electrolytes depend on the microstructure, which can be tuned by crystallization; however, there have been few studies on the crystallization process itself. The properties of solid electrolytes are affected by the phase and crystallite; therefore, controlling the crystallinity or the degree of crystallization could improve properties of the glass–ceramic electrolyte. Therefore, understanding the crystallization kinetics of glass is important for optimizing the heat treatment procedure for crystallization, which remains unclear.

A crystallization analysis was performed using a non-isothermal method, which is easier and faster than the isothermal method. Ozawa reported that isothermal kinetics are simpler than non-isothermal kinetics, but isothermal measurements are only possible when the thermal response time of the measured system is small as compared to the rate of the process. Therefore, a thermoanalytical method should be used, in which the sample is observed under a constant rate of heating or cooling [12].

The crystallization kinetics of the glass system is crucial for understanding the formation of various crystalline phases to understand the stability of glasses and to prepare glass ceramics with desired microstructures and properties

✉ Bong-Ki Ryu
  bkryu@pusan.ac.kr

1   The Institute of Materials Technology, Pusan National University, Busan 46241, South Korea

2   Department of Materials Science and Engineering, Pusan National University, Busan 46241, South Korea

through controlled nucleation and crystallization. The activation energy (E_C) and Avrami index (n) are the important crystallization kinetics of glass ceramics, whose parameters include the temperature range where nucleation can occur, the temperature at which the nucleation rate is at its maximum, and the dependence of the crystal growth mechanism [13]. These parameters can be confirmed by experimental results obtained from non-isothermal thermal analysis studies using the methods suggested by Kissinger and Ozawa [14, 15].

Magnesium oxide as network modifier influences the crystallization and properties of many glass–ceramic systems. Zhang studied the effect of MgO additions and reported the crystallization peak temperatures decreased with increasing MgO additions [16]. Lilensten et al. showed the addition of magnesia has been proved to weaken the network structure of the glasses, thus promoting the precipitation of crystalline phases from the glass matrix [17].

In this study, the crystallization kinetics, such as the E_C and n of $Li_{1+x}Ge_{2-x}Al_xP_3O_{12}$ (LAGP) glass with MgO addition, were investigated under non-isothermal conditions using differential thermal analysis (DTA). After heat treatment of the glass, the crystalline phase was investigated using X-ray diffraction (XRD), and the microstructure of the crystalline phases was observed by scanning electron microscopy (SEM).

2 Experimental details

2.1 Preparation of materials

LAGP glasses doped with MgO were prepared using a conventional melt-quenching method. ($Li_{1.5}Al_{0.5}Ge_{1.5}(PO_4)_3$)-doped MgO, high-purity $NH_4H_2PO_4$ (99.9%), Li_2CO_3 (99.99%), Al_2O_3 (99.99%), GeO_2 (99%), and MgO (99.9%) were used as starting materials to melt the LAGP glass. The batch was mixed in a mortar and then ball-milled for 1 h for homogenization. The mixture was melted in an alumina crucible in an electrically heated furnace under ordinary atmospheric conditions at 500 °C for approximately 30 min to evaporate ammonia, carbonate, and water from the batch and to minimize the tendency for subsequent phosphate volatilization. The temperature was then increased gradually to 1250 °C and maintained for 2 h to homogenize the melt. The melt was quenched by pouring it onto a plate. Based on other studies that reported that the specimen size considerably affects the nucleation barrier, the as-quenched glass was ground and screened with a 44 μm mesh to remove larger particles, thus eliminating this variable [18, 19]. It was then stored in an oven at 100 °C to prevent moisture until it was required for the DTA measurements.

2.2 Measurements and analysis

To determine the kinetic parameters of the samples, DTA (DTG-60H, Shimadzu) measurements were performed using approximately 20 mg of the heat-treated glass powders in an air atmosphere at heating rates of 5, 10, 15, and 20 °C/min up to 800 °C. The DTA results were further analyzed to obtain the crystallization mode and E_C values for the crystallization of each sample using the Kissinger [20], Marotta [21], and Ozawa [12] methods. The slope of each graph was determined using the least squares method.

Heat treatments for the glass–ceramic transformation were realized at 600–650 °C, based on the crystallization peak temperatures (T_P) of the DTA results. The phase analysis and crystallization of the heated samples were examined by XRD (Ultima 4, Rigaku) and SEM (Supra25, Zeiss), respectively. The XRD patterns were recorded using Cu–K radiation in the 2θ range of 10°–80° with a step size of 0.02°. The analytic system showed no systematic error, and the random error was ~2.0%. The crystal phases were analyzed using the XRD patterns.

3 Results and discussion

3.1 Thermal and structural characterization

Figure 1 presents the DTA curves of the glass samples measured at different heating rates. Each glass sample exhibited a single crystallization temperature peak. The characteristic temperatures of the glass (T_C and T_P) decreased with an increasing MgO content because of an increase in the non-bridging oxygen group [22] and increased with an increasing heating rate, as shown in Table 1. This dependence is a result of a higher concentration of nuclei, due to a longer time for
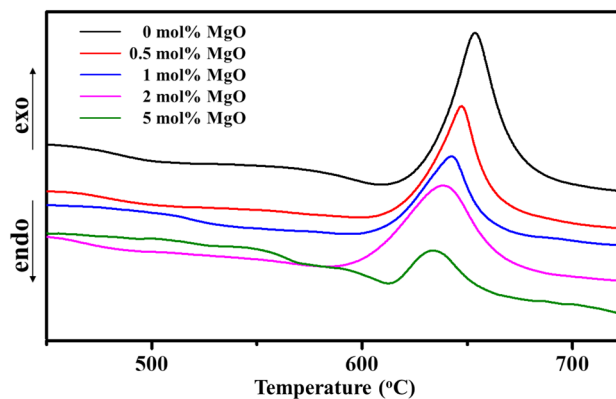

Fig. 1 DTA curves for the glass powder with the different MgO addition at 20 °C/min

Table 1 Crystallization temperatures (T_C, T_P) determined from DTA data obtained at different heating rate

MgO contents	Heating rate (°C/min)	T_C (°C)	T_P (°C)	Heating rate (°C/min)	T_C (°C)	T_P (°C)
0	5	590.9	609.5	15	609.3	636.9
	10	603.2	627.3	20	615.8	648.1
0.5	5	585.9	608.2	15	604.3	635.4
	10	597.4	625.3	20	608.3	643.4
1	5	584.7	608.1	15	594.1	634.8
	10	587.1	623.6	20	598.5	642.4
2	5	582.7	606.9	15	597.3	634.0
	10	587.9	622.7	20	601.4	640.5
5	5	566.5	597.2	15	586.3	620.4
	10	581.7	614.2	20	592.3	630.9
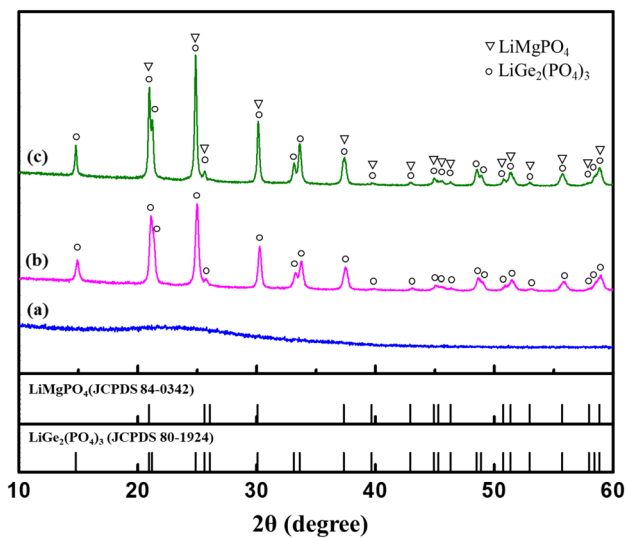
Fig. 2 XRD patterns of the glass samples **a** LAGP without heat treatment, **b** LAGP and **c** LAGP+5 mol% MgO (**b** and **c** sample heat treated to the indicated temperature at a heating rate of 20 °C/min

nucleation at lower heating rates, which causes the crystallization to shift toward lower temperatures. XRD analysis was performed to confirm the nucleation during DTA. Figure 2 presents the XRD patterns of the glass samples heated at 10 °C/min from room temperature to the indicated temperature and held for 2 h. The results confirm that the crystalline phases of $LiGe_2(PO_4)_3$ (JCPDS 80-1924) and $LiMgPO_4$ (JCPDS 84-0342) induce the exothermic peaks in the DTA curves.

3.2 Activation energy for crystallization

To investigate the E_C among the various methods, the Kissinger and Marotta equations were used, and both methods were obtained from the Johnson–Mehl–Avrami (JMA) model [21, 23]. Generally, thermoanalytical technique data

are analyzed by the formal theory of nucleation and growth, and the JMA equation is applied. Equations (1) and (2) express the Kissinger and Marotta equations, respectively.

The Kissinger equation is a common model used to analyze the E_C. The E_C for crystallization was calculated using the Kissinger equation with the crystallization peak temperature from the Differential Scanning Calorimetry (DSC) data. The dependence between the crystallization temperature and heating rate can be described using

$$\ln\left(\frac{\alpha}{T_P^2}\right) = -\frac{E_C}{RT_P} + \text{constant}, \tag{1}$$

where T_P is the crystallization peak temperature, E_C is the activation energy, R is the ideal gas constant (8.3144 J/mol K), and α is the DTA heating rate.

The E_C can be calculated from the slope of $\ln(\alpha/T_P^2)$ versus $1/T_P$, based on which the inverse of E_C can be determined, as shown in Fig. 3. According to Marotta [21, 24, 25], the change in $\ln(T_P^2)$ with α is , expressed as

$$\ln \alpha = -\frac{E_C}{RT_P} + \text{constant}. \tag{2}$$

Therefore, the E_C calculated by the Kissinger model was obtained from the plot of $\ln(\alpha/T_P^2)$ versus $1000/T_P$ and that calculated by the Marotta model was determined from the plot of $\ln\alpha$ versus $1000/T_P$. Figure 3 shows the Kissinger and Marotta plots for the glass at the heating rates of 5, 10, 15, and 20 °C/min. The E_C values were calculated using the slopes of the trend lines, as shown in Table 2. The E_C from the Kissinger and Marotta models for crystallization was 232.55–261.90 kJ/mol and 247.53–276.62 kJ/mol, respectively, as shown in Table 2. The calculated E_C increased with an increasing MgO amount, implying that more energy was required to grow the crystal [26]. Li et at. reported the crystallization activation energy increased with the MgO content, owing to the high viscosity of the glassy phase
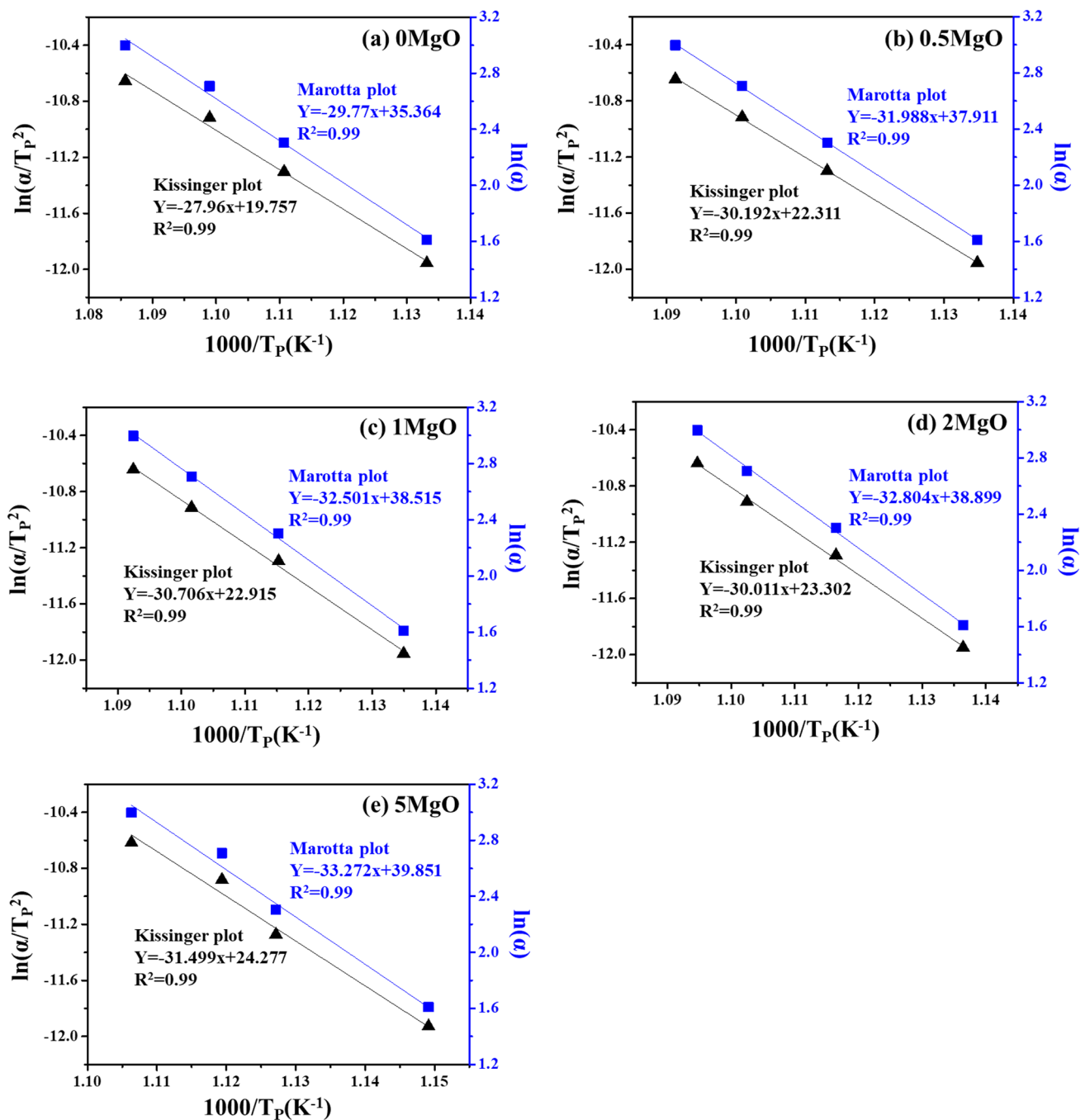
Fig. 3 Kissinger (black triangles) and Marotta (blue squares) plots for the crystallization peaks of LAGP glass samples with **a** 0% MgO, **b** 0.5 MgO, **c** 1% MgO, **d** 2% MgO and **e** 5% MgO addition

appeared at higher MgO contents, and the activation energy was correlated with the viscosity of the glassy phase during the crystal precipitation [27], although more work is required to confirm this.

Considering the mathematical errors and comparing the E_C values calculated by the Kissinger and Marotta models, we found that the values are very similar. In contrast, both values are lower than the E_C obtained by Kun et al. (300 kJ/

mol) [28] using the Kissinger model. However, these authors did not provide information about the particle size of the glassy powders used in their experiments. Moreover, T_P and E_C increase with an increasing particle size [29, 30]. Therefore, as the values of E_C calculated from the Kissinger and Marotta equations depend on T_P, the dependence of these parameters on particle size is also expected. The difference may also be due to the possible difference in the chemical

Table 2 E_C and n for the LAGP glass obtained from the various methods

MgO contents	E_C (kJ/mol)		n	
	Kissinger	Marotta	Ozawa	Augis–Bennett
0	232.55	247.53	3.13	3.40
0.5	251.01	265..98	2.28	2.70
1	255.34	268.31	1.98	2.41
2	257.83	272.71	1.82	1.48
5	261.90	276.62	1.36	1.02
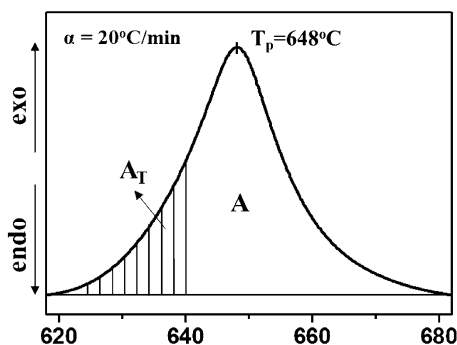
Fig. 4 Area A, between T_i and T_f, and area A_T, between T_i and T, for the crystallization peak

composition of each glass. These differences can be deduced from the discrepancy in the glass transition temperature. This is because, at 5 °C/min, the T_g of the glass we studied was 590 °C, while that of the glass prepared by Kun et al. was 537 °C.

3.3 Avrami Index

Several methods exist for calculating the n from E_C. In this study, n was calculated using the Augis–Bennett and Ozawa equations based on the E_C values.

The fraction of crystallization (χ) at a specific temperature can be determined from the DTA curves [31–33]. The fraction crystallized at a given temperature, T, was obtained by the ratio A_T/A, where A is the total area of the crystallization peak between temperature T_i (where crystallization begins) and temperature T_f (where crystallization is completed). A_T represents the area between T_i and T, as shown schematically in Fig. 4. Figure 5 shows that the χ displayed typical sigmoid curves for the different heating rates. Transformations follow a sigmoidal curve when the transformation rates are low at the beginning and the end of the transformation, but rapid in between. The initial slow rate can be attributed to the time required for the formation and development of a significant number of nuclei in the new phase. During the intermediate period, the transformation is rapid as the

nuclei grow into particles and consume the untransformed phase, while nuclei continue to form. When the transformation approaches completion, few untransformed materials remain for further nucleation, and the production of new particles gradually decreases. Additionally, the previously formed particles begin to contact one another, forming a boundary where growth stops [34–36]. This result indicates that the formation of the crystalline phase proceeded through a combination of nucleation and growth processes.

The Ozawa equation (3) was used to determine n [12, 37].

$$\left[\frac{d \ln(-\ln(1-\chi))}{d \ln\alpha}\right]_T = -n, \tag{3}$$

where χ is the volume fraction crystallized at a fixed temperature, T, and a heating rate, α. From the χ values for each heating rate at a particular temperature, n was determined from the slopes of the trend lines for $\ln(-\ln(1-\chi))$ as a function of $\ln\alpha$, as seen in Fig. 6.

Furthermore, we obtained n using the Augis–Bennett equation:

$$n = \frac{2.5}{\Delta T}\frac{T_P^2}{E/R}, \tag{4}$$

where ΔT is the full width at half maximum of the exothermic peak. Table 2 shows the n calculated using both the Augis–Bennett and Ozawa equations, and the n value was found to be similar to that of other studies [38].

The n is the main parameter used to evaluate the crystal growth mode. According to Ray and Day [39], if $n = 1$, one-dimensional crystal growth occurs, forming acicular crystals. If $n = 2$ and $n = 3$, two-dimensional plate-like crystals and three-dimensional spherical crystal growth occurs, respectively. The n value calculated from the crystallization kinetic approach in this experiment ranged from about 3.13 to 1.36 by Ozawa method. Therefore, the shape of the crystals can range from plate-like to acicular crystals with an increasing MgO content and it is known that the addition of MgO changes the viscosity of the glass, which affects the diffusion of ions, and thereby changes the shape of the crystal phase [40–42]. This conforms with the SEM results shown in Fig. 7, making it possible to validate the kinetic approach through non-isothermal DTA.

4 Conclusions

In this study, the crystallization behavior of LAGP glass with MgO addition was investigated using non-isothermal DTA, XRD, and SEM. The DTA results showed that the current composition exhibited an exothermic T_P at approximately 610 °C. The identification of the crystalline phase by XRD revealed the presence of $LiGe_2(PO_4)_3$ and $LiMgPO_4$.

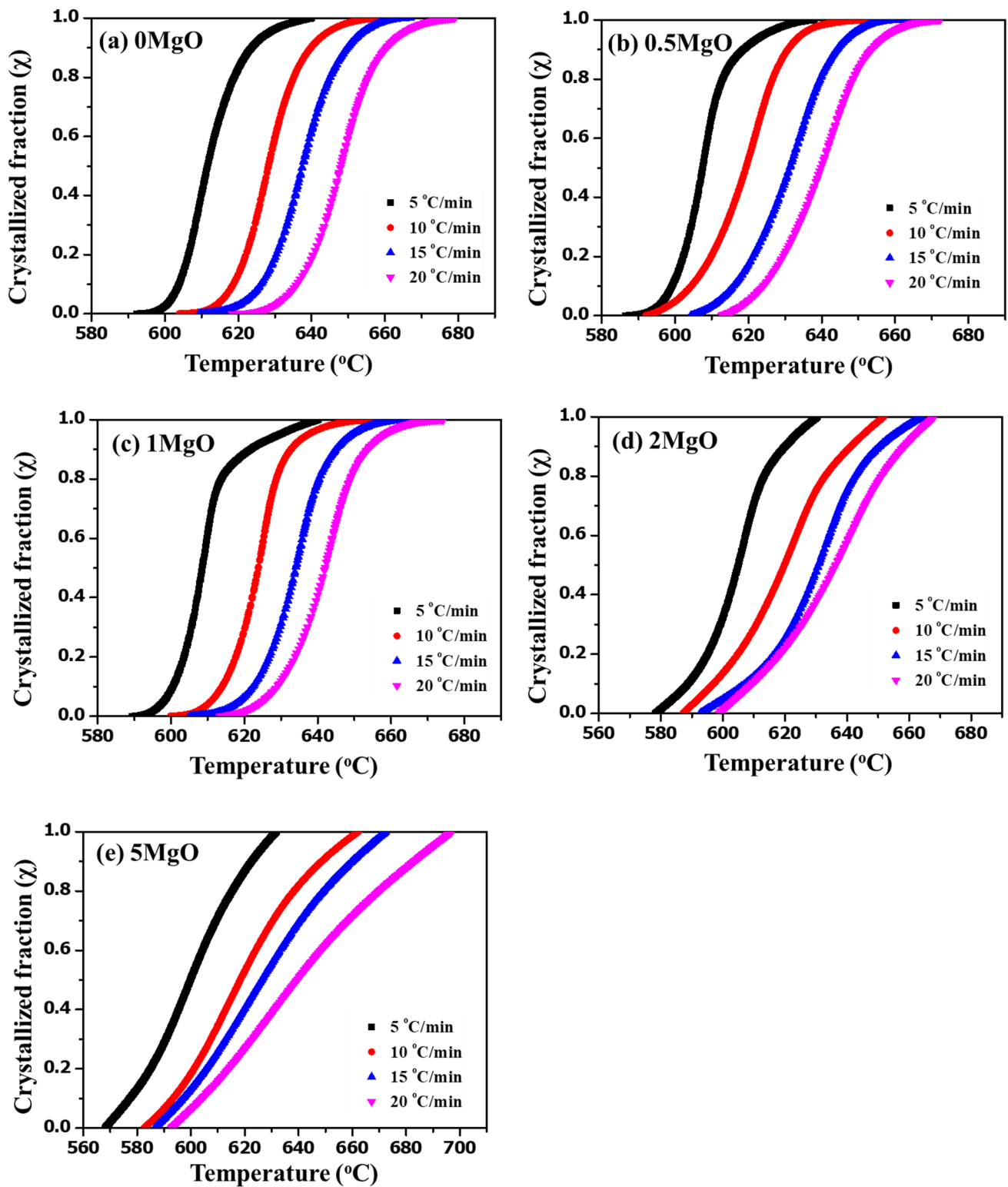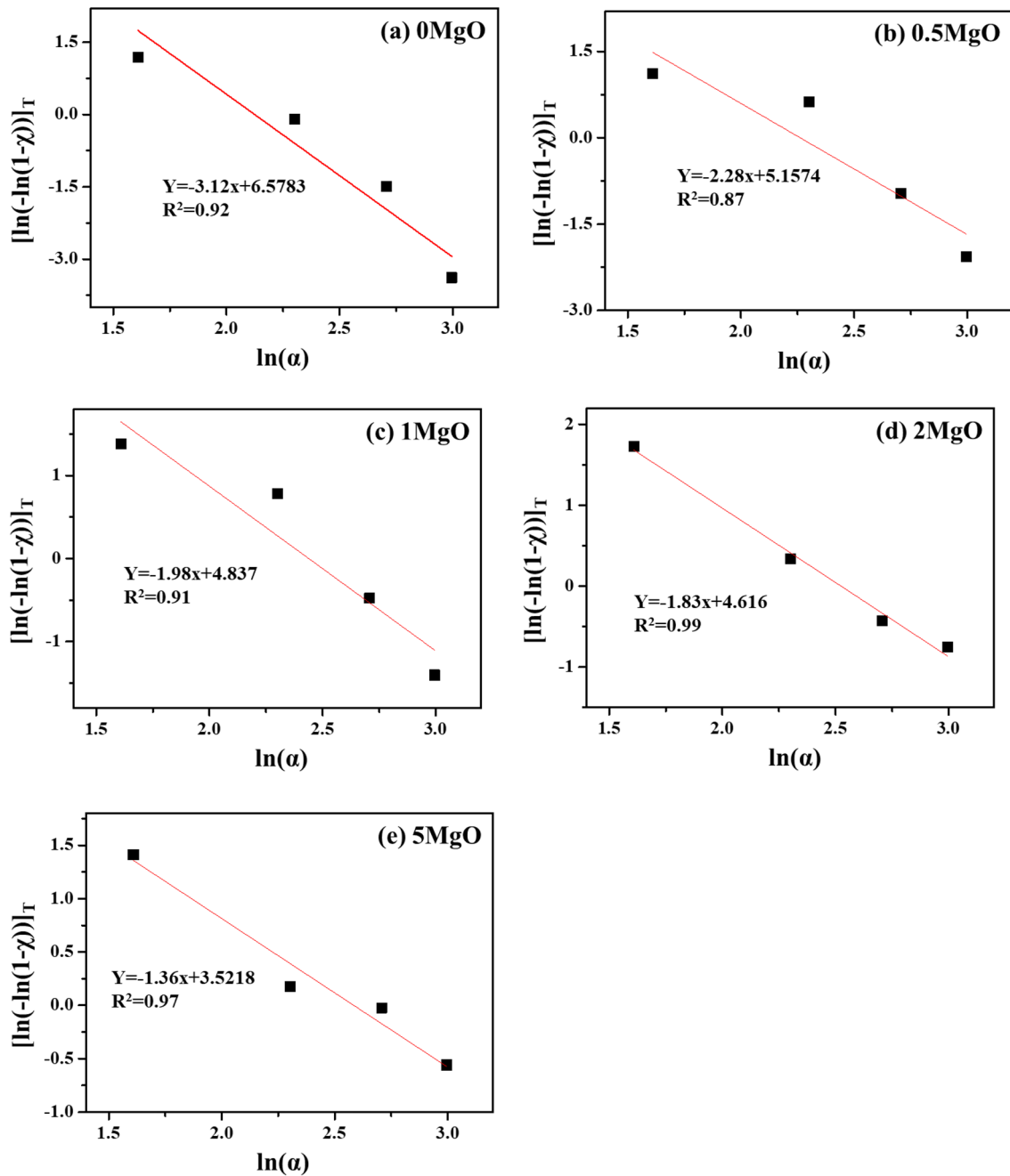**Fig. 5** Crystallized fraction as a function of temperature at different heating rates of LAGP glass samples with **a** 0% MgO, **b** 0.5% MgO, **c** 1% MgO, **d** 2% MgO and **e** 5% MgO addition

Fig. 6 Plot of $\ln(-\ln(1-\chi))$ versus $\ln\alpha$ of LAGP glass samples with **a** 0% MgO, **b** 0.5% MgO, **c** 1% MgO, **d** 2% MgO and **e** 5% MgO addition

The E_C values, as the kinetic parameters, were calculated using both the Kissinger and Marotta methods, and the results were in good agreement. The E_C values calculated by the Kissinger and Marotta models for crystallization were 232.55–261.90 kJ/mol and 247.53–276.62 kJ/mol, respectively. As the MgO content increased, the E_C increased and n decreased. Furthermore, the SEM observations indicated acicular crystal growth.
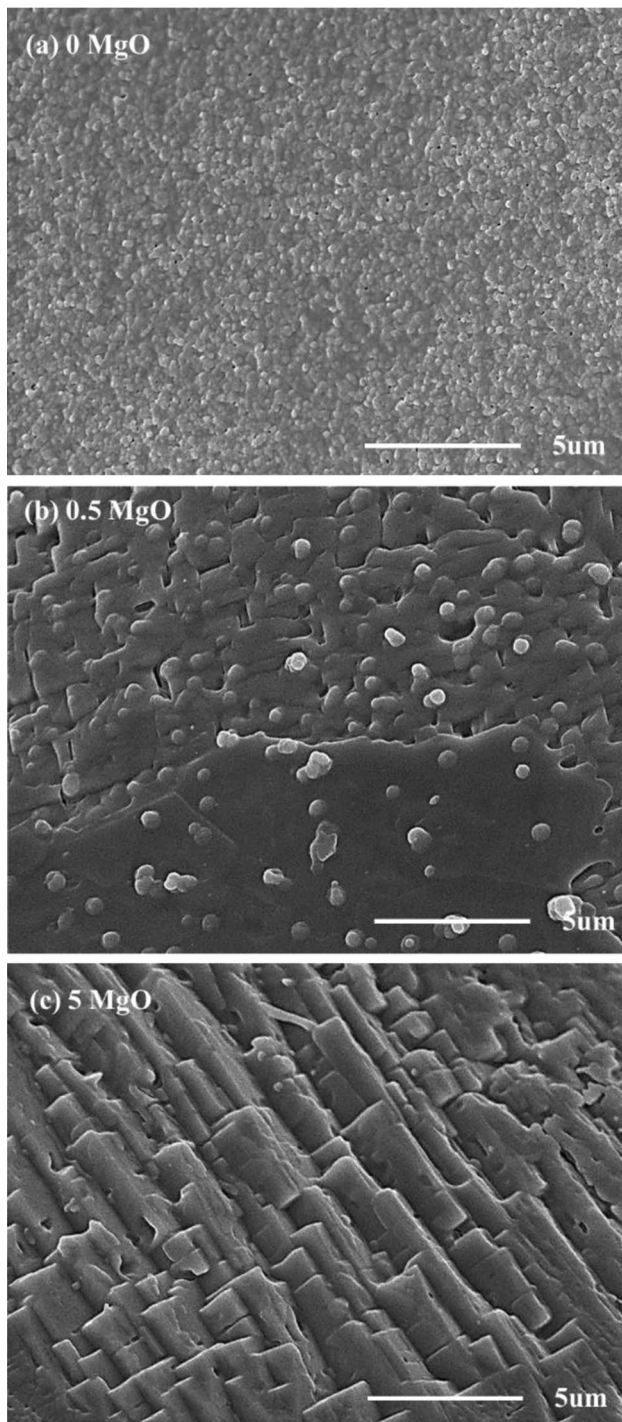
Fig. 7 SEM micrograph of MgO-added LAGP glass crystallization growth at 650 °C for 2 h

References

1. Z. Ding, J. Li, J. Li, C. An, Review-interfaces: key issue to be solved for all solid-state lithium battery technologies. J. Electrochem. Soc. **167**, 070541 (2020)

2. L. He, Q. Sun, C. Chen, J. Oh, J. Sun, M. Li, W. Tu, H. Zhou, K. Zeng, L. Lu, Failure mechanism and interface engineering for NASICON-structured all-solid-state lithium metal batteries. ACS Appl. Mater. Interfaces **11**, 20895–20904 (2019)

3. H. Lim, L. Liu, H. Lee, J. Cha, D. Yoon, B. Ryu, The study on the interface characteristics of solid-stat electrolyte. J. Korean Ceram. Soc. **58**, 373–377 (2021)

4. C. Jung, H. Shim, D. Eum, S. Hong, Challenges and recent progress in $LiNi_xCo_yMn_{1-x-y}O_2$ (NCM) cathodes for lithium ion batteries. J. Korean Ceram. Soc. **58**, 1–27 (2021)

5. H. Nakano, K. Dokko, J. Sugaya, T. Yasukawa, T. Matsue, K. Kanamura, All-solid-state micro lithium-ion batteries fabricated by using dry polymer electrolyte with micro-phase separation structure. Electrochem. Commun. **9**, 2013–2017 (2007)

6. F. Croce, F. Serraino Fiory, L. Persi, B. Scrosati, A high-rate, long-life, lithium nanocomposite polymer electrolyte battery. Electrochem. Solid-State Lett. **4**, 121–123 (2001)

7. K. Takada, M. Tansho, I. Yanase, T. Inada, A. Kajiyama, M. Kouguchi, S. Kondo, M. Watanabe, Lithium ion conduction in $LiTi_2(PO_4)_3$. Solid State Ion. **139**, 241–247 (2001)

8. T. Abe, M. Ohtsuka, F. Sagane, Y. Iriyama, Z. Ogumi, Lithium-ion transfer at the interface between lithium-ion conductive ceramic electrolyte and liquid electrolyte—a key to enhancing the rate capability of lithium-ion batteries. J. Electrochem. Soc. **151**, 2151–2154 (2004)

9. A. Hayashi, T. Konishi, K. Tadanaga, M. Tatsumisago, Formation of electrode–electrolyte interface by lithium insertion to $SnS–P_2S_5$ negative electrode materials in all-solid-state cells. Solid State Ion. **177**, 2737–2740 (2006)

10. X. Chen, P. Vereecken, Solid and solid-like composite electrolyte for lithium ion batteries: engineering the ion conductivity at interfaces. Adv. Mater. Interfaces **6**, 1800899 (2019)

11. K. Heo, J. Im, J. Lee, S. Kim, J. Kim, J. Lim, High-rate blended cathode with mixed morphology for all solid-state Li-ion batteries. J. Electrochem. Sci. Technol. **11**, 282–290 (2020)

12. T. Ozawa, Kinetics of non-isothermal crystallization. Polymer **12**, 150–158 (1971)

13. J. Sestak, The applicability of DTA to the study of crystallization kinetics of glasses. Phys. Chem. Glasses. **15**, 137–140 (1974)

14. H. Yinnon, D.R. Uhlmann, Applications of thermoanalytical techniques to the study of crystallization kinetics in glass-forming liquids, part I: Theory. J. Non-cryst. Solids **54**, 253–275 (1983)

15. H.E. Kissinger, Reaction kinetics in differential thermal analysis. Anal. Chem. **29**, 1702–1706 (1957)

16. Y. Zhang, Z. Luo, T. Liu, X. Hao, Z. Li, A. Lu, MgO-doping in the $Li_2O–ZnO–Al_2O_3–SiO_2$ glass–ceramics for better sealing with steel. J. Non-cryst. Solids **405**, 170–175 (2014)

17. L. Lilensten, Q. Fu, B.R. Wheaton, A.J. Credle, R.L. Stewart, J.T. Kohli, Kinetic study on lithium-aluminosilicate (LAS)

glass-ceramics containing MgO and ZnO. Ceram. Int. **40**, 11657–11661 (2014)

18. H. Kim, The crystallization kinetics of CaO–MgO–Al$_2$O$_3$–sio$_2$ glass system using thermal analysis. J. Korean Ceram. Soc. **29**, 9–14 (1992)

19. J. Sestak, Use of phenomenological kinetics and the enthalpy versus temperature diagram (and its derivative-DTA) for a better understanding of transition processes in glasses. Thermochim. Acta **208**(281), 175–190 (1996)

20. H.E. Kissinger, Variation of peak temperature with heating rate in differential thermal analysis. J. Res. Natl. Stand. **57**, 217–221 (1956)

21. A. Marotta, A. Buri, Kinetics of devitrification and differential thermal analysis. Thermochim. Acta **25**, 155–160 (1978)

22. I. Jlassi, N. Sdiri, H. Elhouichet, Electrical conductivity and dielectric properties of MgO doped lithium phosphate glasses. J. Non-cryst. Solids. **466–467**, 45–51 (2017)

23. J. Malek, The applicability of Johnson–Mehl–Avrami model in the thermal analysis of the crystallization kinetics of glasses. Thermochim. Acta. **267**, 61–73 (1955)

24. A. Marotta, A. Buri, F. Branda, Nucleation in glass and differential thermal analysis. J. Mater. Sci. **16**, 341–344 (1981)

25. A. Marotta, S. Saiello, F. Branda, A. Buri, Activation energy for the crystallization of glass from DDTA curves. J. Mater. Sci. **17**, 105–108 (1982)

26. M. Kang, S. Kang, Influence of Al$_2$O$_3$ additions on the crystallization mechanism and properties of diopside/anorthite hybrid glass–ceramics for LED packaging materials. J. Cryst. Growth **326**, 124–127 (2011)

27. B. Li, Y. Guo, J. Fang, Effect of MgO addition on crystallization, microstructure and properties of glass–ceramics prepared from solid wastes. J. Alloys Compd. **881**, 159821 (2021)

28. H. Kun, W. Yanhang, Z. Chengkui, Z. Huifeng, L. Yonghua, C. Jiang, H. Bin, M. Juanrong, Influence of Al$_2$O$_3$ additions on crystallization mechanism and conductivity of Li$_2$O–Ge$_2$O–P$_2$O$_5$ glass–ceramics. Physica B Condens. Matter. **406**, 2947–2950 (2011)

29. C.S. Ray, D.E. Day, W. Huang, K. Narayan, T.S. Cull, K.F. Kelton, Non-isothermal calorimetric studies of the crystallization of lithium disilicate glass. J. Non-cryst. Solids. **204**, 1–12 (1996)

30. M. Fathollahi, S. Pourmortazavi, S. Hossenini, Particle size effects on thermal decomposition of energetic material. J. Energ. Mater. **26**, 52–69 (2008)

31. A. Arora, E.R. Shaaban, K. Singh, O.P. Pandey, Non-isothermal crystallization kinetics of ZnO–BaO–B$_2$O$_3$–SiO$_2$ glass. J. Non-cryst. Solids. **354**, 3944–3951 (2008)

32. M. Ghasemzadeh, A. Nemati, A. Nozad Golikand, Z. Hamnabard, S. Baghshahi, Utilization of DTA in the determination of a crystallization mechanism in transparent glass–ceramics with a nanocrystalline structure. Inorg. Nano-Met. Chem. **41**, 561–570 (2011)

33. C.R. Chang, J.H. Jean, Crystallization kinetics and mechanism of low-dielectric, low-temperature, cofirable CaO–B$_2$O$_3$–SiO$_2$ glass-ceramics. J. Am. Ceram. Soc. **82**, 1725–1732 (1999)

34. M. Avrami, Kinetics of phase change: I. General theory. J. Chem. Phys. **7**, 1103–1112 (1939)

35. M. Avrami, Kinetics of phase change: II. Transformation-time relations for random distribution of nuclei. J. Chem. Phys. **8**, 212–224 (1940)

36. M. Avrami, Kinetics of phase change: III. Granulation, phase change and microstructure. J. Chem. Phys. **9**, 177–184 (1941)

37. X.J. Xu, C.S. Ray, D.E. Day, Nucleation and crystallization of Na$_2$O · 2CaO · 3SiO$_2$ glass by differential thermal analysis. J. Am. Ceram. Soc. **74**, 909–914 (1991)

38. A. Das, M. Goswami, M. Krishnan, Crystallization kinetics of Li$_2$O–Al$_2$O$_3$–GeO$_2$–P$_2$O$_5$ glass–ceramics system. J. Therm. Anal. Calorim. **131**, 2421–2431 (2018)

39. C.S. Ray, D.E. Day, *Ceramic Transactions Nucleation and Crystallization in Liquids and Glasses* (The American Ceramic Society, Ohio, 1993), pp. 207–223

40. Z. Lu, J. Lu, X. Li, G. Shao, Effect of MgO addition on sinterability, crystallization kinetics, and flexural strength of glass-ceramics from waste materials. Ceram. Int. **42**, 3452–3459 (2016)

41. J. Li, Y. Guo, G. Li, J. Chen, C. Li, Y. Zou, Investigation into the role of MgO in the synthesis of MAPO-11 large single crystals. Microporous Mesoporous Mater. **79**, 79–84 (2005)

42. S.M. Salman, S.N. Salama, H. Darwish, E.A. Mahdy, The role of MgO on the structural properties of CaO–Na$_2$O(MgO)–P$_2$O$_5$–CaF$_2$–SiO$_2$ derived glass ceramics. Ceram. Int. **36**, 55–61 (2010)